Constraints on Weak Supernova Kicks from Observed Pulsar Velocities

Reinhold Willcox[1,2] , Ilya Mandel[1,2,3] , Eric Thrane[1,2] , Adam Deller[2,4] , Simon Stevenson[2,4] , and
Alejandro Vigna-Gómez[5]
[1] School of Physics and Astronomy Monash University, Clayton, VIC 3800, Australia; reinhold.willcox@monash.edu
[2] The ARC Centre of Excellence for Gravitational Wave Discovery—OzGrav, Australia
[3] Institute of Gravitational Wave Astronomy and School of Physics and Astronomy, University of Birmingham, Birmingham, B15 2TT, UK
[4] Centre for Astrophysics and Supercomputing, Swinburne University of Technology, Hawthorn, VIC 3122, Australia
[5] DARK, Niels Bohr Institute, University of Copenhagen, Jagtvej 128, DK-2200, Copenhagen, Denmark

Abstract

Observations of binary pulsars and pulsars in globular clusters suggest that at least some pulsars must receive weak natal kicks at birth. If all pulsars received strong natal kicks above $50\,km\,s^{-1}$, those born in globular clusters would predominantly escape, while wide binaries would be disrupted. On the other hand, observations of transverse velocities of isolated radio pulsars indicate that only $5 \pm 2\%$ have velocities below $50\,km\,s^{-1}$. We explore this apparent tension with rapid binary population synthesis modeling. We propose a model in which supernovae with characteristically low natal kicks (e.g., electron-capture supernovae) only occur if the progenitor star has been stripped via binary interaction with a companion. We show that this model naturally reproduces the observed pulsar speed distribution and without reducing the predicted merging double neutron star yield. We estimate that the zero-age main-sequence mass range for noninteracting progenitors of electron-capture supernovae should be no wider than $\approx 0.2\,M_\odot$.

Unified Astronomy Thesaurus concepts: Neutron stars (1108); Pulsars (1306); Binary pulsars (153); Supernovae (1668)

1. Introduction

The observed single pulsar population is characterized by typical speeds of hundreds of $km\,s^{-1}$, generally attributed to large natal kicks due to asymmetric mass ejection during supernovae (SNe; Hobbs et al. 2005; Burrows 2013; Verbunt et al. 2017; Deller et al. 2019). Such large kicks are consistent with simulations of core-collapse supernovae (CCSNe; Wongwathanarat et al. 2012; Müller 2020). On the other hand, the existence of pulsars in globular clusters, where escape velocities can be $\lesssim 50\,km\,s^{-1}$, points to the need for a subpopulation of pulsars with low kicks (e.g., Sigurdsson 2003). Meanwhile, natal kicks that disrupt the binary inhibit the formation of double neutron stars (DNSs) (e.g., Beniamini & Piran 2016; Vigna-Gómez et al. 2018). Therefore, at least some fraction of neutron stars (NSs) must receive low natal kicks.

Theoretically, low kicks ($\lesssim 30\,km\,s^{-1}$) are often associated to electron-capture supernovae (ECSNe) and ultra-stripped supernovae (USSNe). USSNe only occur as the second SN in very tight binaries with minimal mass loss and almost never disrupt the binary; thus, we do not consider them further as they do not contribute to the velocity distribution of isolated pulsars (Tauris et al. 2015). ECSNe are thought to arise from a subset of the super-asymptotic giant branch (sAGB) stars, which span a zero-age main-sequence (ZAMS) mass range of ≈ 6.5–$12\,M_\odot$, though the precise ZAMS mass range for ECSN progenitors is highly uncertain (see Doherty et al. 2017 for a review).

In this paper, we use the COMPAS[6] rapid binary population synthesis code (Stevenson et al. 2017; Vigna-Gómez et al. 2018) in order to reconcile the paucity of observed low-velocity pulsars with the need for a population of NSs with low natal kicks. We find that by restricting low natal kicks to occur only

in stars that have previously transferred mass to a binary companion, our model reproduces the observed fraction of low-velocity isolated pulsars, without inhibiting the DNS yield. We interpret this as an upper limit on the ZAMS mass range for effectively single progenitors of ECSNe, while leaving the channel for stripped stars unaffected.

Our proposal builds on indications that ECSNe from single stars are less common than initially thought (Miyaji et al. 1980; Nomoto 1984; Poelarends et al. 2008), but could be enhanced in binaries because envelope stripping by Roche-lobe overflow onto a companion suppresses second dredge-up (Podsiadlowski et al. 2004; van den Heuvel 2010; Ibeling & Heger 2013; Dall'Osso et al. 2014; Poelarends et al. 2017).

In Section 2, we discuss the data set of pulsar velocities observed with very long baseline interferometry and the associated selection effects. In Section 3, we describe our population synthesis prescriptions. We present the results in Section 4. In Section 5, we discuss the caveats of our analysis and its implications for stellar evolution models.

2. Data and Selection Effects

The data used in this study are astrometric measurements of isolated pulsars obtained with very long baseline interferometry (VLBI). We use exclusively VLBI measurements rather than the larger data sets based on pulsar timing or dispersion measure because VLBI provides precise measurements and we aim to avoid concerns about systematic uncertainty in other pulsar velocity measurements (Deller et al. 2019).

We select a total of 81 pulsars from a variety of studies, primarily Deller et al. (2019) but also Bailes et al. (1990), Fomalont et al. (1999), Chatterjee et al. (2001), Brisken et al. (2002, 2003), Dodson et al. (2003), Chatterjee et al. (2004, 2009), Deller et al. (2009), and Kirsten et al. (2015). We remove millisecond pulsars, pulsars known to be in binaries, and pulsars

---

6 https://compas.science/

in globular clusters in order to obtain a relatively homogeneous data set of pulsars whose velocities are primarily set by SN natal kicks (and any previous isolated binary evolution) rather than dynamics. Some of the apparently single pulsars may still be in binaries, as binaries with orbital periods much longer than the observational baseline are challenging to detect.

The data for each pulsar contain sets of bootstrapped fits for the parallax, position, and proper motion. We treat the fits as posterior samples. We reweigh them by applying a prior on the parallax to be above 0.05 mas, i.e., the distance to be below 20 kpc, consistent with Galactic pulsars, as well as a prior on the transverse velocities to be less than 2000 km s^{-1}, to exclude anomalously large values.

We extract an intrinsic transverse velocity relative to the pulsar's local standard of rest (LSR) by correcting for Galactic rotation and the motion of the Sun. We assume a flat Galactic rotation curve, with constant speed 230 km s^{-1} (Bhattacharjee et al. 2014), and take solar velocity $(U, V, W)_\odot = (11.1, 244, 7.25)$ km s^{-1} (Schönrich et al. 2010). This correction assumes that the LSR velocity vector of the pulsar today is similar to its LSR at birth, which relies on the assumption of insignificant acceleration in the Galactic potential. This is valid for very young or slow-moving pulsars, but is not justified, e.g., for a 20 Myr pulsar moving at 500 km s^{-1}, which would have traveled for ∼10 kpc in the absence of external forces. However, only pulsars with high velocities (comparable to or larger than the local Galactic rotational velocity) will be impacted, so this is not expected to affect our analysis of low-velocity pulsars. A bigger concern is that the data were not collected in a manner intended to be a complete survey. Indeed, Deller et al. (2019) note that their sample focused specifically on systems at high Galactic latitudes, which could lead to a paucity of low-velocity pulsars. However, the distributions of characteristic ages and heights off the Galactic plane are indistinguishable between our sample and the broader sample of all isolated, nonmillisecond pulsars in the ATNF pulsar catalog.[7]

It is also conceivable that pulsars with low velocities are naturally fainter and harder to detect because of some correlation between their formation physics and an observational characteristic relevant to radio detectability that is not yet understood (Sigurdsson 2003). We test for this possible bias by examining the correlation between pulsar transverse velocities and distances. A Malmquist bias favors detecting only radio-bright pulsars at greater distances. Therefore, if low-velocity pulsars tend to be fainter in the radio band, we should see a positive correlation between distance and transverse velocity. While there is a mild correlation between distance and velocity, we confirmed that its magnitude is fully consistent with arising from the construction of transverse velocity as a product of proper motion and distance, with significant uncertainties in the distance (typically of order 20%). We therefore see no evidence for a selection effect against low-velocity pulsars once this correlation is accounted for. Further, we find that the correlation between the transverse velocities and heights of the pulsars out of the Galactic plane is no greater than the correlation between the transverse velocities and pulsar distances, which further supports the absence of a significant bias due to preferentially observing pulsars at high Galactic latitudes. Figure 1 shows the transverse velocity distributions at the low end of our catalog.

---

[7] https://www.atnf.csiro.au/research/pulsar/psrcat/
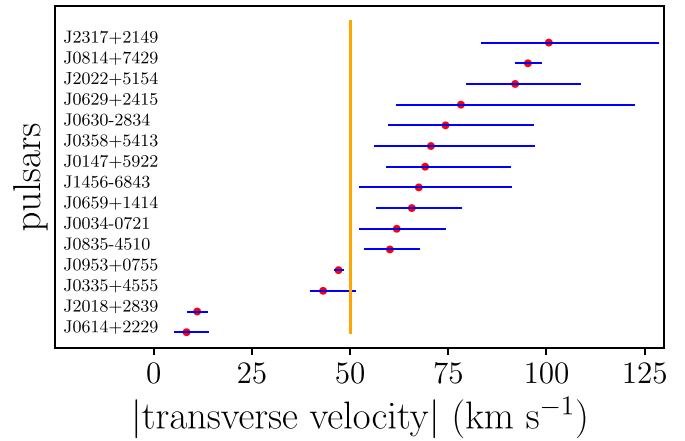
Figure 1. Transverse velocity medians and 5%–95% confidence intervals for the 15 lowest-velocity pulsars in our sample. Defining 50 km s^{-1} as the boundary between low- and high-speed pulsars is convenient since no pulsar shows strong support on both sides of this value.

3. Methods

We use the COMPAS rapid binary population synthesis code (Team COMPAS: Riley et al. 2021) to generate synthetic pulsar transverse velocity distributions for several different SN kick prescriptions. We simulate a total of 10^6 binaries per prescription, with primary ZAMS mass drawn from the Kroupa (2001) initial mass function between 5 and 150 $M_\odot$, mass ratio drawn uniformly from 0.01 to 1, and semimajor axis distributed uniformly in the log between 0.01 and 1000 au (Öpik 1924). Here, very wide, noninteracting binaries represent the single star population. All binaries are initially circularized ($e_0 = 0$) and use solar metallicity $Z_\odot = 0.0142$ (Asplund et al. 2009). Unless otherwise specified, we follow the default COMPAS prescriptions (Stevenson et al. 2017; Vigna-Gómez et al. 2018; Vinciguerra et al. 2020; Team COMPAS: Riley et al. 2021).

We assume that a star with a helium core mass above 2.25 $M_\odot$ at the base of the asymptotic giant branch will undergo CCSN once the mass of its carbon-oxygen core reaches the threshold set in Equation (75) of Hurley et al. (2000), in which we replace the Chandrasekhar mass with 1.38 $M_\odot$ (Belczynski et al. 2008). We set the CCSN remnant mass according to the Fryer et al. (2012) delayed prescription. If the helium core mass is between 1.6 and 2.25 $M_\odot$ at the base of the asymptotic giant branch and the carbon-oxygen core mass subsequently reaches 1.38 $M_\odot$, the star is assumed to form an NS with mass 1.26 $M_\odot$ in an ECSN.

We consider a variety of different kick prescriptions, all based on the following "fiducial" prescription. Natal kicks for pulsars formed in CCSNe (hereafter, CC-pulsars, and similarly for EC-pulsars) are drawn directly from the observed pulsar velocity distribution. To obtain a 3D kick magnitude for the CC-pulsars, we randomly draw a velocity sample from the union of the transverse velocity posterior distributions of pulsars in our catalog, selecting only among values of at least 50 km s^{-1}, and divide by a random projection coefficient under the assumption of an isotropic viewing angle.

This is in contrast to the COMPAS default CCSN kick prescription (which uses the Hobbs et al. 2005 Maxwellian model) and other evolution codes, which draw from parameterized, analytical distributions, because these distributions differ from the observations at high velocities. However, this difference is due directly to the assumed shape of the natal kick distribution. The bulk of the isolated pulsar population have

very high speeds $\gtrsim 300\,\mathrm{km\,s^{-1}}$, much larger than typical pre-SN orbital velocities,

$$v_{\mathrm{orb}} \approx 42\mathrm{km\,s^{-1}} \left(\frac{M}{20M_\odot} \right)^{1/2} \left(\frac{a}{10\mathrm{au}} \right)^{-1/2},$$

where M is the total binary mass and a is the separation of a circular binary. Consequently, the pulsar is nearly always unbound, with a final speed dominated by the magnitude of the natal kick, with some scatter on the order of v_{orb}. By drawing CCSN kicks directly from the observations, we are able to focus on the poorly understood low-velocity regime.

In the FIDUCIAL prescription (henceforth abbreviated as FID), all EC-pulsars have natal kick magnitudes drawn from a Maxwellian with $\sigma_{\mathrm{1D\,rms}} = 30\,\mathrm{km\,s^{-1}}$.

All SN natal kicks are applied isotropically in the progenitor rest frame (see Bray & Eldridge 2018 and Giacobbo & Mapelli 2020, who investigate anisotropic kicks). If the SN disrupts the binary through a combination of symmetric mass loss (the Blaauw kick; Blaauw 1961) and the natal kick, the speed of the NS is given by its asymptotic speed once it has escaped the gravitational potential of the companion. If the binary remains intact, the speed of the NS is given by the sum in quadrature of its speed in the center-of-mass frame and the binary velocity relative to the LSR, if any. We then project the NS speed onto the plane of the sky assuming an isotropically distributed viewing angle to obtain a transverse velocity prediction. NSs in wide binaries with orbital periods above 10 yr are categorized together with isolated NSs as "apparently isolated"; varying the period threshold between 10 and 100 yr has a negligible impact. Wide binary pulsars comprise $\sim 20\%$ of the total apparently isolated NS population, immediately following the SN, in all our prescriptions. This fraction is a few times higher than the estimated fraction of pulsars in wide binaries obtained by Antoniadis (2021; $\lesssim 10\%$), who considered observability through Gaia and radio pulsar surveys under a very simple model of binary properties (see also Igoshev & Perets 2019). This discrepancy is in part due to the fact that our 20% estimate does not account for the amount of time that a pulsar is observable in a wide binary, which could be disrupted by a second supernova. It would be interesting to compare the properties of wide binaries predicted by our models against observations through a similar modeling of selection effects.

ECSNe are the primary source of low-velocity pulsars in our models, so we consider variations on the FID prescription described above that impact ECSNe. In the first variation, KICK: 1 km s^{-1} (K1), we reduce the natal kicks of ECSNe down to a Maxwellian with $\sigma_{\mathrm{1D\,rms}} = 1\,\mathrm{km\,s^{-1}}$, motivated in part by hydrodynamical simulations (Gessner & Janka 2018). The second variation, NO WIDE ECSNE (NW), flags and ignores ECSNe in noninteracting binaries, allowing for ECSNe only in stars that previously lost mass through Roche-lobe overflow. The final variation, NO WIDE ECSNE, KICK: 1 km s^{-1} (NW-K1), combines the first and second variations. A list of variations is given in Table 1.

4. Results

In Figure 2, we compare the transverse velocity cumulative distribution functions (CDFs) of apparently isolated NSs from the FID (a) and NW (b) prescriptions to those of the observed pulsars. Each observed transverse velocity CDF (black) is constructed by randomly sampling one posterior transverse velocity sample per pulsar. The spread in these CDFs indicates the uncertainty in the velocity measurements. Each synthetic CDF (colored) is constructed by randomly drawing as many velocities as the total number of observed pulsars $N_P = 81$ from the modeled population. Their spread indicates the impact of small number statistics. The CDFs match at velocities $\gtrsim 400\,\mathrm{km\,s^{-1}}$ (both panels), validating the use of the CCSN prescription used in this study.

Meanwhile, the mismatch between the modeled and observed velocity distributions in (a) at low velocities indicates that the FID prescription overpredicts the number of low-velocity pulsars. The preferred NW prescription (b) reduces the disagreement in the low-velocity regime by removing NSs from ECSNe in noninteracting binaries.

We devise a statistic in order to quantify the goodness of fit between model and data. For a specified cutoff velocity v_{cut}, let f_{low} represent the fraction of low-speed pulsars with transverse velocity $\leqslant v_{\mathrm{cut}}$, as predicted by a given model variation. We choose a value of $v_{\mathrm{cut}} = 50\,\mathrm{km\,s^{-1}}$. While this value is somewhat ad hoc, it serves to differentiate between high kicks, which disrupt binaries and eject pulsars from globular clusters, and low kicks, which do not. Let N_{slow} be the number of observed pulsars with velocity $\leqslant v_{\mathrm{cut}}$ out of N_P. The probability of observing N_{slow} low-velocity pulsars out of N_P is described by the binomial distribution. The probability of observing N_{slow} pulsars or fewer is thus given by

$$P(\leqslant N_{\mathrm{slow}}|f_{\mathrm{low}}) = \sum_{i=0}^{N_{\mathrm{slow}}} C_i^{N_P} (f_{\mathrm{low}})^i (1 - f_{\mathrm{low}})^{N_P - i}. \quad (1)$$

In practice, N_{slow} is not known precisely due to the measurement uncertainty in observed pulsar transverse velocities, so it is marginalized out. Under the null hypothesis that the data are drawn from the model variation, $P(\leqslant N_{\mathrm{slow}}|f_{\mathrm{low}})$ is uniformly distributed, allowing us to rule out any variations that yield very small or very large values for $P(\leqslant N_{\mathrm{slow}}|f_{\mathrm{low}})$.

$P(\leqslant N_{\mathrm{slow}}|f_{\mathrm{low}})$ is plotted in Figure 3 in black. The simulated f_{low} values are shown as colored vertical lines; the uncertainty due to the finite simulated population is within the width of the lines. The null hypothesis is in tension with the data when a model, specified by f_{low}, intersects the black curve outside the indicated $\pm 2\sigma$ interval (see Table 1 for exact values of $P(\leqslant N_{\mathrm{slow}}|f_{\mathrm{low}})$).

Figure 3(a) shows f_{low} values calculated after including low-velocity pulsars from both CCSNe and ECSNe. Model variations with f_{low} values that cross the $P(\leqslant N_{\mathrm{slow}}|f_{\mathrm{low}})$ curve below the -2σ threshold overproduce low-velocity pulsars from a combination of ECSNe and CCSNe. This is the case for the FID and K1 variations. Meanwhile, both variations that mask out ECSNe in noninteracting binaries cross well above the threshold and cannot be ruled out.

In order to distinguish the relative importance of ECSNe kicks and low-velocity CCSNe kicks, in Figure 3(b), we consider an alternative population in which we include only EC-pulsars as low-velocity pulsars. Explicitly, we assume that all CC-pulsars are given very large kicks. Now, only the K1 model still crosses below the -2σ cutoff, so it is the only model that can be confidently ruled out on the basis that it overproduces low-velocity pulsars from ECSNe alone. The low-velocity EC-pulsars in this model predominantly come from binaries disrupted by Blaauw kicks, though $\sim 30\%$ are in intact, very wide binaries.

Table 1
List of Model Names and Descriptions Considered in This Study, Along with the $P(\leqslant N_{\rm slow}|f_{\rm low})$ Value Derived If We Include and Exclude CC-pulsars, and the Yield of DNSs Merging in Hubble Time per $10^6\ M_\odot$ of Star Formation

Model	$P(\leqslant N_{\rm slow}\|f_{\rm low})$ Including Slow Pulsars from CCSNe	$P(\leqslant N_{\rm slow}\|f_{\rm low})$ Excluding Slow Pulsars from CCSNe	Merging DNS Yield per $10^6\ M_\odot$	Variation
FIDUCIAL (FID)	0.0049 ✗	0.069 ✓	7.1 ± 0.3	⋯
KICK: 1 km s^{-1} (K1)	0.0003 ✗	0.011 ✗	8.1 ± 0.3	All ECSN kicks are reduced to 1 km s^{-1}
NO WIDE ECSNE (NW)	0.2716 ✓	0.950 ✓	7.1 ± 0.3	Noninteracting ECSN progenitors are removed
NO WIDE ECSNE, KICK: 1 km s^{-1} (NW-K1)	0.1741 ✓	0.918 ✓	7.5 ± 0.3	Noninteracting ECSN progenitors are removed, other ECSN kicks are reduced to 1 km s^{-1}

Note. Models with $P(\leqslant N_{\rm slow}|f_{\rm low}) < 0.023$ overproduce slow pulsars at a rate inconsistent with observations at a 2σ level, as indicated by the check and cross marks.

(a) Fiducial (FID)


(b) No Wide ECSNe (NW)
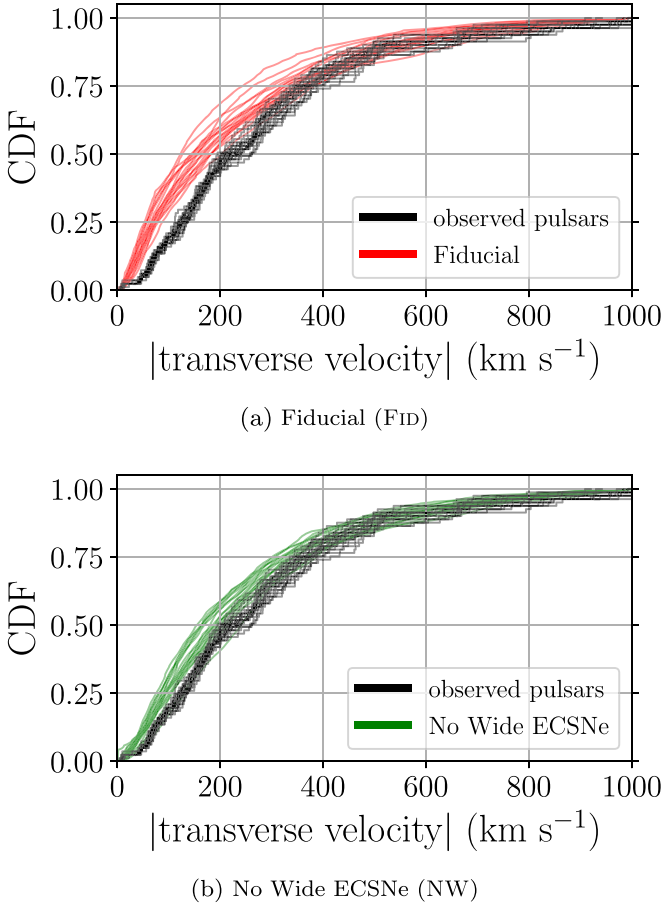
Figure 2. CDFs of the observed pulsar transverse velocities (black curves) and those predicted by the model variations (colored curves). Families of CDFs are drawn to illustrate uncertainty (see Section 4). The FID variation (a) overproduces low-speed pulsars ($\lesssim 50$ km s^{-1}). The NW variation (b) improves the match at low speeds by removing ECSN progenitors that did not transfer mass onto a binary companion.

The FID model now falls just within the 2σ confidence interval and cannot be confidently ruled out. However, the high production of low-velocity EC-pulsars alone indicates a likely tension with observations. The two models that mask noninteracting ECSNe, NW, and NW-K1, now nearly cross above the $+2\sigma$ level, suggesting that they significantly underproduce low-velocity pulsars. Since we have intentionally removed CC-pulsars here, this merely suggests that some fraction of low-velocity pulsars may be contributed by CC-pulsars.

5. Discussion

We model supernova progenitors using binary population synthesis in order to self-consistently test NS natal kick models against observed pulsar transverse velocities. We find that our FID variation overproduces low-speed, apparently isolated pulsars in comparison with observations. This discrepancy can be resolved if supernovae that produce low-speed, apparently isolated NSs are suppressed in wide binaries when the NS progenitor did not experience Roche-lobe overflow onto a companion.

If ECSNe indeed produce weak natal kicks, this provides a constraint for models of sAGB stars that might otherwise be expected to undergo ECSN. In the FID variation, single stars with ZAMS mass in the range ≈ 7.5–$8.1\,M_\odot$ yield ECSNe. This constitutes $\sim 13\%$ of NS progenitors, assuming a Kroupa (2001)

(a) Including slow pulsars from CCSNe

(b) Assuming fast kicks from CCSNe
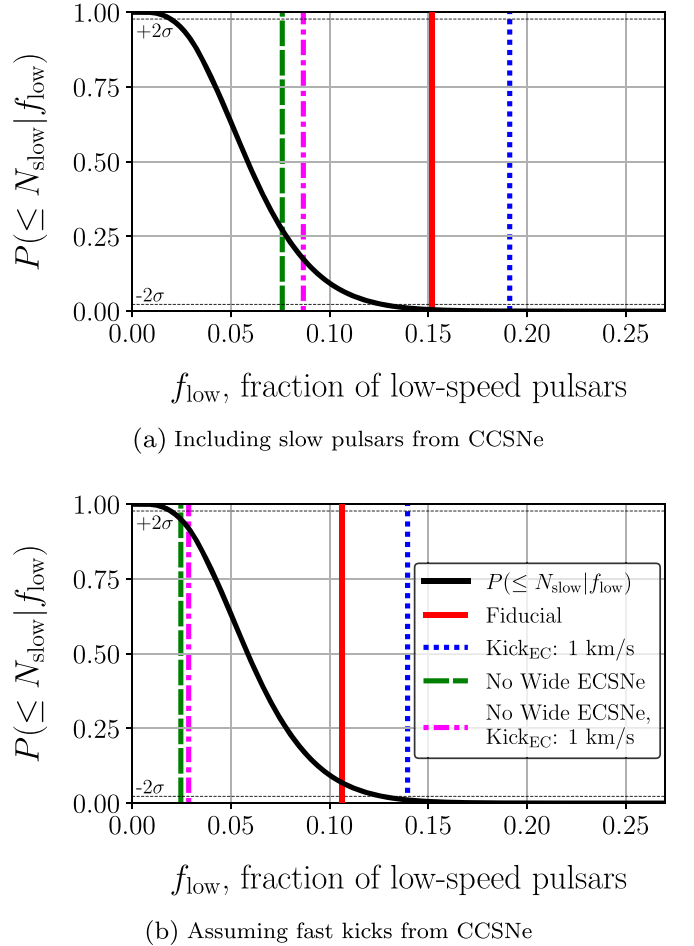
Figure 3. Probability $P(\leqslant N_{\rm slow}|f_{\rm low})$ (black curve) that the observations would contain no more than the observed number $N_{\rm slow}$ of low-speed ($\leqslant 50$ km s^{-1}) pulsars out of $N_P = 81$, given a true fraction $f_{\rm low}$ of slow pulsars (see the text). Also plotted are model predictions for the slow pulsar fraction $f_{\rm low}$ (colored, vertical lines). In panel (a), $f_{\rm low}$ includes slow pulsars from both CCSNe and ECSNe. In panel (b), $f_{\rm low}$ includes only slow EC-pulsars. Models that cross the black curve outside the $\pm 2\sigma$ confidence bounds are in tension with observations (though see the text for caveats).

initial mass function and a ZAMS mass range extending to $20\,M_\odot$ for NS progenitors. Figures 2 and 3 suggest that a contribution of no more than a few percent from noninteracting EC-pulsars would be more consistent with observations. This would require a reduction in the width of the ZAMS mass range for ECSN progenitors to $\lesssim 0.2\,M_\odot$, or removing this possibility altogether, as in our NW and NW-K1 models. This is consistent with Doherty et al. (2017), who predict an ECSN progenitor ZAMS mass range of ≈ 9.5–$9.7\,M_\odot$ at $Z_\odot$ (and indeed a width of $\approx 0.2\,M_\odot$ across all metallicities), as well as Tarumi et al. (2021) who find a similarly narrow mass range for ECSN progenitors from dwarf galaxy Sr abundances (Hirai et al. 2019). Our results are qualitatively similar at $Z_\odot/10$. We do not distinguish between ECSNe and low-mass iron-core CCSNe in our models (Podsiadlowski et al. 2004); an increased yield from the latter, if they produce comparably low kicks, would then require a proportional reduction in the former. We have not considered here the possibility that accretion-induced collapse of white dwarfs may lead to weakly kicked NSs, as the models for this channel remain very uncertain (Nomoto & Kondo 1991; Ruiter et al. 2019; Wang & Liu 2020).

Although no ECSN progenitors have been observationally confirmed, some candidate populations have been proposed that, if validated, would help to constrain the nature of ECSNe in single stars (O'Grady et al. 2020). Indeed, Hiramatsu et al. (2021) propose that SN 2018zd was an ECSN from a single sAGB star based on the low energy and chemical profile of the light curve. However, we find this to be unlikely if ECSNe are indeed very rare in single stars. Additionally, the light curves for stripped ECSNe may be very short, rendering detection especially challenging, which could explain the dearth of ECSN candidates. A possible alternative to reducing the ZAMS mass range for producing ECSNe from single stars would be reducing the observability of the remnant as a young radio pulsar.

We obtain an additional constraint on natal kicks by considering their effect on DNS merger rates. Galactic double neutron star and gravitational-wave observations indicate a local DNS merger rate of 430^{+280}_{-130} Gpc^{-3} yr^{-1} (Pol et al. 2020) and 320^{+490}_{-240} Gpc^{-3} yr^{-1} (Abbott et al. 2021), respectively. Given a local star formation rate of $1.5 \times 10^7 \, M_\odot$ Gpc^{-3} yr^{-1} (Madau & Dickinson 2014), this implies a yield of $\sim$25 merging DNSs per $10^6 \, M_\odot$ of star formation. Our models predict a lower DNS yield of seven to eight merging DNSs per $10^6 \, M_\odot$ of star formation (see Table 1). However, some of the locally merging DNSs formed at higher redshifts when the star formation rate was higher, so this yield is not inconsistent with observations. Removing ECSNe in wide binaries does not reduce the merging DNS yield since such systems are very unlikely to form DNSs merging within a Hubble time.

Our analysis is limited by the size of the observational data set and by the possibility of selection effects in choosing which pulsars are followed up with VLBI. A complete VLBI follow-up within a predetermined volume could address both concerns.

ORCID iDs

Reinhold Willcox ● https://orcid.org/0000-0003-0674-9453
Ilya Mandel ● https://orcid.org/0000-0002-6134-8946
Eric Thrane ● https://orcid.org/0000-0002-4418-3895
Adam Deller ● https://orcid.org/0000-0001-9434-3837
Simon Stevenson ● https://orcid.org/0000-0002-6100-537X
Alejandro Vigna-Gómez ● https://orcid.org/0000-0003-1817-3586

References

Abbott, R., Abbott, T. D., Abraham, S., et al. 2021, ApJL, 913, L7
Antoniadis, J. 2021, MNRAS, 501, 1116
Asplund, M., Grevesse, N., Sauval, A. J., & Scott, P. 2009, ARA&A, 47, 481
Astropy Collaboration, Price-Whelan, A. M., Sipőcz, B. M., et al. 2018, AJ, 156, 123
Astropy Collaboration, Robitaille, T. P., Tollerud, E. J., et al. 2013, A&A, 558, A33
Bailes, M., Manchester, R. N., Kesteven, M. J., Norris, R. P., & Reynolds, J. E. 1990, MNRAS, 247, 322
Belczynski, K., Kalogera, V., Rasio, F. A., et al. 2008, ApJS, 174, 223
Beniamini, P., & Piran, T. 2016, MNRAS, 456, 4089
Bhattacharjee, P., Chaudhury, S., & Kundu, S. 2014, ApJ, 785, 63
Blaauw, A. 1961, BAN, 15, 265
Bray, J. C., & Eldridge, J. J. 2018, MNRAS, 480, 5657
Brisken, W. F., Benson, J. M., Goss, W. M., & Thorsett, S. E. 2002, ApJ, 571, 906
Brisken, W. F., Thorsett, S. E., Golden, A., & Goss, W. M. 2003, ApJL, 593, L89
Burrows, A. 2013, RvMP, 85, 245
Chatterjee, S., Brisken, W. F., Vlemmings, W. H. T., et al. 2009, ApJ, 698, 250
Chatterjee, S., Cordes, J. M., Lazio, T. J. W., et al. 2001, ApJ, 550, 287
Chatterjee, S., Cordes, J. M., Vlemmings, W. H. T., et al. 2004, ApJ, 604, 339
Dall'Osso, S., Piran, T., & Shaviv, N. 2014, MNRAS, 438, 1005
Deller, A. T., Goss, W. M., Brisken, W. F., et al. 2019, ApJ, 875, 100
Deller, A. T., Tingay, S. J., Bailes, M., & Reynolds, J. E. 2009, ApJ, 701, 1243
Dodson, R., Legge, D., Reynolds, J. E., & McCulloch, P. M. 2003, ApJ, 596, 1137
Doherty, C. L., Gil-Pons, P., Siess, L., & Lattanzio, J. C. 2017, PASA, 34, e056
Fomalont, E. B., Goss, W. M., Beasley, A. J., & Chatterjee, S. 1999, AJ, 117, 3025
Fryer, C. L., Belczynski, K., Wiktorowicz, G., et al. 2012, ApJ, 749, 91
Gessner, A., & Janka, H.-T. 2018, ApJ, 865, 61
Giacobbo, N., & Mapelli, M. 2020, ApJ, 891, 141
Harris, C. R., Millman, K. J., van der Walt, S. J., et al. 2020, Natur, 585, 357
Hirai, Y., Wanajo, S., & Saitoh, T. R. 2019, ApJ, 885, 33
Hiramatsu, D., Howell, D. A., Van Dyk, S. D., et al. 2021, NatAs, 5, 903
Hobbs, G., Lorimer, D. R., Lyne, A. G., & Kramer, M. 2005, MNRAS, 360, 974
Hunter, J. D. 2007, Comput Sci Eng, 9, 90
Hurley, J. R., Pols, O. R., & Tout, C. A. 2000, MNRAS, 315, 543
Ibeling, D., & Heger, A. 2013, ApJL, 765, L43
Igoshev, A. P., & Perets, H. B. 2019, MNRAS, 486, 4098
Kirsten, F., Vlemmings, W., Campbell, R. M., Kramer, M., & Chatterjee, S. 2015, A&A, 577, A111
Kroupa, P. 2001, MNRAS, 322, 231
Madau, P., & Dickinson, M. 2014, ARA&A, 52, 415
Manchester, R. N., Hobbs, G. B., Teoh, A., & Hobbs, M. 2005, AJ, 129, 1993
Miyaji, S., Nomoto, K., Yokoi, K., & Sugimoto, D. 1980, PASJ, 32, 303
Müller, B. 2020, LRCA, 6, 3
Nomoto, K. 1984, ApJ, 277, 791
Nomoto, K., & Kondo, Y. 1991, ApJL, 367, L19
O'Grady, A. J. G., Drout, M. R., Shappee, B. J., et al. 2020, ApJ, 901, 135
Öpik, E. 1924, Publications of the Tartu Astrofizica Observatory, 25, 1
Podsiadlowski, P., Langer, N., Poelarends, A. J. T., et al. 2004, ApJ, 612, 1044
Poelarends, A. J. T., Herwig, F., Langer, N., & Heger, A. 2008, ApJ, 675, 614
Poelarends, A. J. T., Wurtz, S., Tarka, J., Cole Adams, L., & Hills, S. T. 2017, ApJ, 850, 197
Pol, N., McLaughlin, M., & Lorimer, D. R. 2020, RNAAS, 4, 22
Ruiter, A. J., Ferrario, L., Belczynski, K., et al. 2019, MNRAS, 484, 698
Schönrich, R., Binney, J., & Dehnen, W. 2010, MNRAS, 403, 1829
Sigurdsson, S. 2003, in ASP Conf. Ser., 302, Radio Pulsars, ed. M. Bailes, D. J. Nice, & S. E. Thorsett (San Francisco, CA: ASP), 391
Stevenson, S., Vigna-Gómez, A., Mandel, I., et al. 2017, Nat. Commun, 8, 14906
Tarumi, Y., Suda, T., van de Voort, F., et al. 2021, MNRAS, 505, 3755

---

[8] COMPAS is freely available at http://github.com/TeamCOMPAS/COMPAS.

Tauris, T. M., Langer, N., & Podsiadlowski, P. 2015, MNRAS, 451, 2123
Team COMPAS: Riley, J., Agrawal, P., Barrett, J. W., et al. 2021, arXiv:2109.10352
van den Heuvel, E. P. J. 2010, NewAR, 54, 140
Van Rossum, G., & Drake, F. L. 2009, Python 3 Reference Manual (Scotts Valley, CA: CreateSpace)
Verbunt, F., Igoshev, A., & Cator, E. 2017, A&A, 608, A57

Vigna-Gómez, A., Neijssel, C. J., Stevenson, S., et al. 2018, MNRAS, 481, 4009
Vinciguerra, S., Neijssel, C. J., Vigna-Gómez, A., et al. 2020, MNRAS, 498, 4705
Wang, B., & Liu, D. 2020, Res. Astron. Astrophys, 20, 135
Wongwathanarat, A., Janka, H.-T., & Müller, E. 2012, in IAU Symp. 279, Death of Massive Stars: Supernovae and Gamma-Ray Bursts, ed. P. Roming, N. Kawai, & E. Pian (Cambridge: Cambridge Univ. Press), 150